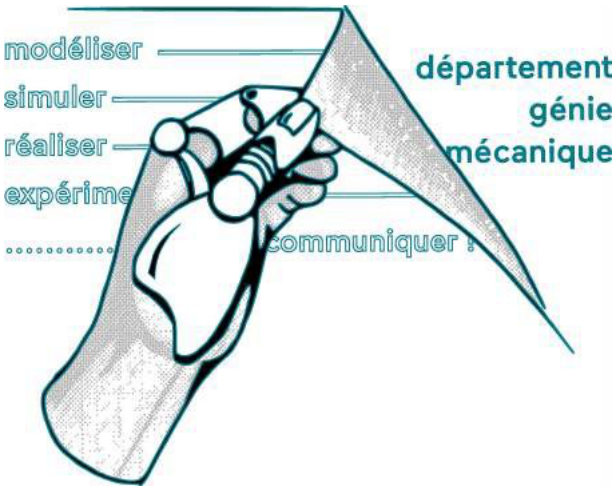


# RESEARCH PROJECTS

## STUDENTS OF THE DEPARTMENT OF MECHANICAL ENGINEERING

## 2024-2025

ABSTRACT

# Analysis of biaxial compression tests using Hopkinson bars

L. P. Dewaele, T. Fix, B. Durand

TER M1 2024-2025
Final defence of research projects

école normale supérieure paris—saclay

**TER M1 2024-2025**
FINAL DEFENCE OF RESEARCH PROJECTS
March 25, 2025, Gif-sur-Yvette, France

# Analysis of biaxial compression tests using Hopkinson bars

**Léo-Paul Dewaele*, Thomas Fix†, Bastien Durand◇**
**Ecole Normale Supérieur Paris Saclay**

* Mechanical Engineering
e-mail: leo-paul.dewaele@ens-paris-saclay.fr

† Mechanical Engineering
e-mail: thomas.fix@ens-paris-saclay.fr

◇ LMPS
e-mail: bastien.durand@ens-paris-saclay.fr

**KEYWORDS :** dynamic biaxial compression; Hopkinson bars; image correlation.

## ABSTRACT

The study of dynamic material behavior under complex loading conditions is crucial to understand the mechanical responses of materials. Even more when these materials are subjected to extreme environments, such as impacts, explosions, and high-strain-rates [1]. Uniaxial compression tests using the Hopkinson bars have been widely employed to characterize materials at high strain rates. However many real-world applications involve multiaxial stress states that cannot be accurately represented by uniaxial testing. Consequently, there is a growing need to develop experimental techniques capable of inducing multiaxial compression at high strain rates. These tests could be used to better recreate the stress conditions encountered in aerospace, structural, and defense applications.

Biaxial compression testing using Hopkinson bars presents challenges, including the need for precise force balance, synchronized loading, and accurate strain measurement in multiple directions [2, 3]. Recent progress in experimental mechanics has led to modifications of the traditional Hopkinson bar set-up. These modifications often include additional impact mechanisms, cruciform samples and multiple bars [4]. These innovations aim to reproduce the stress states observed in real-world scenarios while maintaining the accuracy and repeatability of Hopkinson bar experiments.

Our study presents an experimental approach for achieving biaxial compression using a modified Hopkinson bar system. A bored part filled with oil is used to balance forces and synchronize loads along the two axis of the sample. The methodology, implementation challenges, and potential applications of this technique will be discussed. Special attention will be given to the assembly and positioning of the oil-based system within the modified Hopkinson bar set-up.

The experimental set-up consists of four pairs of steel bars arranged in a cross shape and two corner deflectors. A single projectile is used to ensure optimal synchronization [2], unlike other designs that require four electromagnetic devices for precise timing [4]. With our set-up [2], an air cannon fires the projectile from above, striking the first deflector, which distributes the impact onto four outward-moving bars. A second set of deflectors redirects the incident wave toward the oil cavities device and the sample (see figure 1).

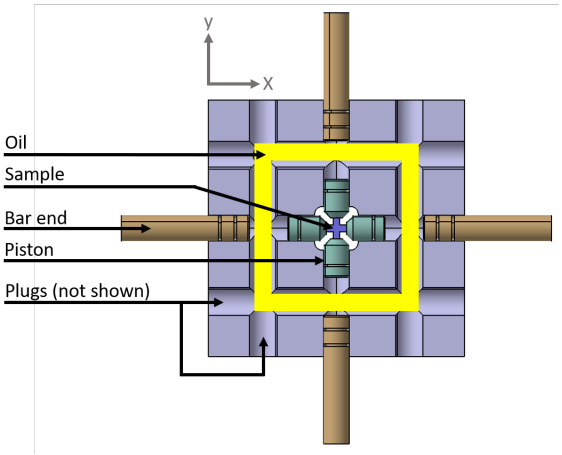


**Figure 1**: Oil cavities device

When the four waves reach the hydraulic device, four pistons press on the oil simultaneously, transferring force to four inner pistons in contact with the cross-shaped sample. The oil enables an equal force distribution due to fluid equilibrium. The diameter of the bars is 10 mm and they reach several meters per second during the test effective duration - less than one milisecond.

For measurements, a standard Hopkinson bar device uses a single strain gauge per bar to capture incident and reflected waves. In this modified set-up, two strain gauges are placed, one after the second deflector and another before the piston. This allows accurate tracking of wave propagation and applied forces on the sample. A high-speed camera records the sample deformation, with speckled paint patterns enabling digital image correlation. Data from the strain gauges and camera are synchronized to ensure precise analysis of the impact and material response. After processing the results, the relationship between the applied force, which is considered as the average of the measured forces on the four axes, and the shrinkages of the cruciform sample along its two main directions is compared to a finite element model generated using Abaqus.

Although the experimental results are subjected to noise, they remained close to the analytical elastic curve. In contrast, classical Hopkinson tests do not allow for accurate elasticity measurements due to alignment issues. Further investigations with additional data and sample sizes would be valuable to assess repeatability, enhance the experimental process and refine the impact force.

## REFERENCES

[1] Sudheera, Y S Rammohan, Pradeep M S. Split Hopkinson Pressure Bar Apparatus for Compression Testing: A Review. *Elsevier*, 2016.

[2] P. Quillery, B. Durand, M. Huang, K. Seck, H. Zhao. Dynamic Biaxial Compression Tests Using 4 Symmetric Input Hopkinson Bars. *Experimental Mechanics*, 2024.

[3] Philippon S, Voyiadjis GZ, Faure L, Lodygowski A, Rusinek A, Chevrier P, Dossou E (2011). A Device enhancement for the dry sliding friction coefficient measurement between steel 1080 and vascomax with respect to surface roughness changes. Exp Mech 51(3):337–358

[4] Kanghua Jin, Lin Qi, Huaipu Kang, Yazhou Guo, Yulong Li. A novel technique to measure the biaxial properties of materials at high strain rates by electromagnetic Hopkinson bar system. *International Journal of Impact Engineering*, 2022.

# Thermal parametric optimization applied to the design of electric machines

A. Nachawati, D. Zandvliet, L. Laurent, F. Louf

TER M1 2024-2025 Final defence of research projects

école normale supérieure paris–saclay

**TER M1 2024-2025**
FINAL DEFENCE OF RESEARCH PROJECTS
April 8, 2025, Gif-sur-Yvette, France

# Thermal parametric optimization applied to the design of electric machines

**Ahmed Nachawati[1], Daniel Zandvliet[1], Luc Laurent[2], François Louf[3]**

[1] Department of Mechanical Engineering
École normale supérieure Paris-Saclay
4 avenue des Sciences 91190 Gif-sur-Yvette
e-mail: ahmed.nachawati@ens-paris-saclay.fr
e-mail: daniel.zandvliet@ens-paris-saclay.fr

[2] Laboratoire de Mécanique des Structures et des Systèmes Couplés
Conservatoire national des arts et métiers
292 rue Saint-Martin 75003 Paris
e-mail: luc.laurent@lecnam.net

[3] Laboratoire de Mécanique Paris-Saclay
École normale supérieure Paris-Saclay
4 avenue des Sciences 91190 Gif-sur-Yvette
e-mail: francois.louf@ens-paris-saclay.fr

**KEYWORDS:** Optimization; Thermal problem; Electrical machine.

Current climate change is driving the exploration of more energy-efficient technologies. Electrical machines, whether operating as motors or as generators, are widespread across most companies, playing a major role in industrial and commercial applications. Electrical machines consume approximately 67% of the total electricity used. At a national scale, electrical machines represent nearly 50% of overall electricity consumption in France. It highlights the need to improve the energy efficiency in order to reduce their environmental impact [1]. The performance of an electrical motor is determined by its electromagnetic, thermal, and mechanical behavior: the electromagnetic behavior determines the motor's power output, heat must be managed to avoid demagnetization, and the structure must withstand mechanical stresses. Despite this interdependence, relatively few studies have focused on the multiphysical optimization of electrical machines [2]. While mechanical and magnetic aspects have been widely studied, thermal effects have received comparatively less attention. In this study, we focused exclusively on stationary thermal effects, as thermal changes significantly impact magnetic properties.

We used a 2D model and studied only an angular section of the stator, since the full geometry can be rebuilt thanks to the periodicity of the structure. The studied domain consists of a coil, which is the only heat source we consider, a magnet, and a ferromagnetic structure filling the gap between both elements, to guide the magnetic flux. We need to modify the geometry of the stator in order to evacuate the heat (see Figure 1a). We defined a hole in the stator, which diameter and position were the parameters to be optimized. The convective fluid flowing through this hole evacuates the calories so as to reduce the temperature inside the stator. After the problem was established, we implemented the thermal equations of the system on NGSolve, an environment of python, which is specialized in finite element method computations. To approach the optimization problem, there are several minimization possible. Here, the objective function we defined is the minimization of the average temperature in the magnet area, in order to limit the risk of demagnetization. We also added geometric constraints to prevent the hole from going outside the ferromagnetic structure. We implemented a weight function that penalizes the objective function when these constraints are not satisfied. In a first approach, the parameters to be

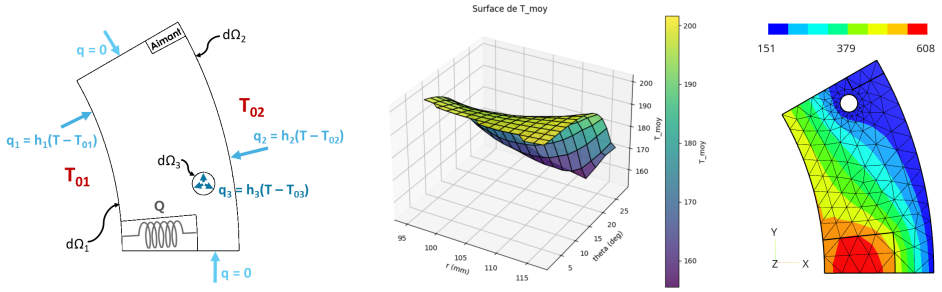


(a) (b) (c)

**Figure 1**: (a) diagram of the thermal problem, (b) surface of the mean temperature, (c) visualization of the optimized solution

optimized were only the polar coordinates (r, $\theta$), determining the position of the hole, and the diameter was fixed to 5mm. Using only two parameters made it easy to get graphs we could analyse (see Figure 1b and 1c). We implemented a brute-force optimization to have a first approximation of the minimization and then applied a parametric optimization with the Nelder-Mead method to accurately and efficiently determine the parameters to be optimized with a choice of weighting between the objective function and the arbitrary constraint. In a second phase, we allowed all three parameters to vary, and a problem appeared: the larger the diameter of the hole, the lower the temperature inside the stator and the smaller the iron surface area. The iron surface ensures the magnetostatic performance of the stator, but when it becomes too thin, the ferromagnetic structure may saturate and no longer conduct the magnetic flux effectively [3]. To resolve this problem, we added a constraint to find an equilibrium between minimizing the temperature and maximizing the iron surface area.

Our results indicates that the thermal effects have an impact on the efficiency of an electrical machine. The Nelder-Mead parametric optimization proposed a more efficient solution that is still close to the brute optimization, which confirms the choice of this computational tool. However, this study reveals that the multi-physical aspect is important to obtain solutions in accordance with the reality. Future research on multiple holes or on topology optimization could be assessed in order to discover better solutions. Further multi-physics studies including mechanical, magnetic, and thermal aspects would be necessary for a more realistic analysis.

## REFERENCES

[1] M.-L. Idoughi. *Extraction de modèles thermiques simplifiés des machines électriques pour une utilisation dans les systèmes de propulsion des véhicules électriques hybrides.* INP Toulouse, 2011

[2] X. Xiao, J. Zhu, Y. Guo, D. Li. Coupled Thermal-Magnetic Analysis of Permanent Magnet Machines Considering Temperature Effects on Magnetic Properties. *Journal of Magnetism and Magnetic Materials, 2019.*

[3] S. Bance, J. Fischbacher, A. Kovacs, H. Oezelt, F. Reichel, T. Schrefl. *Thermal activation in permanent magnets.* arXiv, 2016.

# 4D analysis of the mechanical behavior of a multilayered material imaged by synchrotron radiation

**L. Amitrano, A. Aran, F. Hild**

TER M1 2024-2025
Final defence of research projects

école normale supérieure paris–saclay

**TER M1 2024-2025**
FINAL DEFENCE OF RESEARCH PROJECTS
April 8, 2025, Gif-sur-Yvette, France

# 4D analysis of the mechanical behavior of a multilayered material imaged by synchrotron radiation

**L. Amitrano*, A. Aran*, F. Hild◇**

École normale supérieure Paris-Saclay
4 avenue des Sciences, 91190 Gif-sur-Yvette, France
*Department of Mechanical Engineering
e-mail:{louis.amitrano,axelle.aran}@ens-paris-saclay.fr
◇LMPS – Laboratoire de Mécanique Paris-Saclay
e-mail: {francois.hild}@ens-paris-saclay.fr

**KEYWORDS:** Damage; Digital Volume Correlation; Gauss-Newton algorithm; Multilayered material

## Background and objectives

Recently, the aeronautical industry has been using composite materials (around 50%) to lighten aircraft structures. In contrast to metallic solutions, composite structures require protection from direct and indirect effects of lightning strikes. This protection is usually made out of highly conductive materials such as copper or silver. It is then complemented by multilayered paint for aesthetic layers. The main objective of this coating is to preserve the essential properties, namely, shield the aircraft against external aggression while allowing it to be adapted to the industry new demands. The aim of this project is to analyse the behaviour and mechanical properties of such multilayered system imaged during a tensile test within the European synchrotron radiation facility. 4D displacement fields were measured using digital volume correlations and analysed to extract relevant mechanical information.

## Methods

In order to determine all the information related to the deformation of the tested material, such as displacement and strain fields under loading, first, a mesh made of four noded tetraedra (T4) is prepared. Once the mesh is generated, a MATLAB code is needed to correctly position it on the imaged reference configuration via a Gauss-Newton algorithm. This algorithm provides the three translations and three rotations required for proper positioning. As a result, the mesh accurately aligns with the reference volume, particularly along the notch, which is the critical part of the sample because of the induced strain concentration. Next, Digital Volume Correlation (DVC), which consists in minimising, in the least-squares sense [1], the differences between the reference image and the deformed image corrected by the displacement field $\underline{u}(\underline{x}, t)$, is run. Since a finite element mesh is used, the DVC code determines the nodal displacements for each analysed configuration. Six deformed images are registered for a loading range from 40 N to 230 N. The DVC process is carried out in two steps. First, incremental correlations are run, which involve correlating 3D images sequentially. This step serves as an initialization for the next DVC analyses. The second step consists in performing direct correlations, where each deformed image is registered with the same reference image (acquisition at 0 N).

## Results

The results obtained from DVC proved to be interesting. The DVC analyses enabled the displacement and strain fields to be measured within the multilayered material. In addition, the volumetric DVC residuals are observed. These residuals enable for a visual representation of the damaged areas, in particular close to the notch root for the various layers. Figure 1 shows the longitudinal displacement field corresponding to an applied force of 190 N.

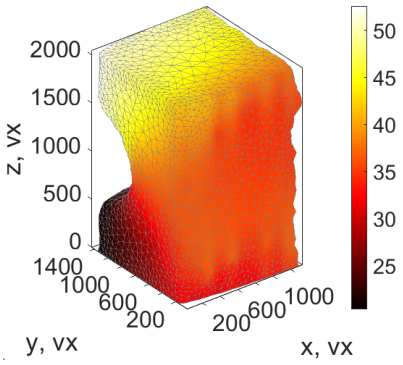


**Figure 1**: Longitudinal displacement field (expressed in voxel) for an applied loading of 190 N. The physical size of 1 voxel is 1.45 µm

A separation of the different layers of the material is performed to focus exclusively on the paint, with the aim of quantifying the strain levels up to severe conditions. A section is performed within the paint layer (figure 2(b)). Figure 2(a) shows the corresponding grey level residuals from the DVC calculation. The analysis of the residuals does not reveal any cracking. Figure 2(c) displays the longitudinal strain within the same section. The paint withstands a strain of at least 3%, which is the maximum level under a loading of 190 N. The maximum strain in the paint for a loading of 230 N is 5%, at which point the onset of cracking is observed on the gray level residual map.

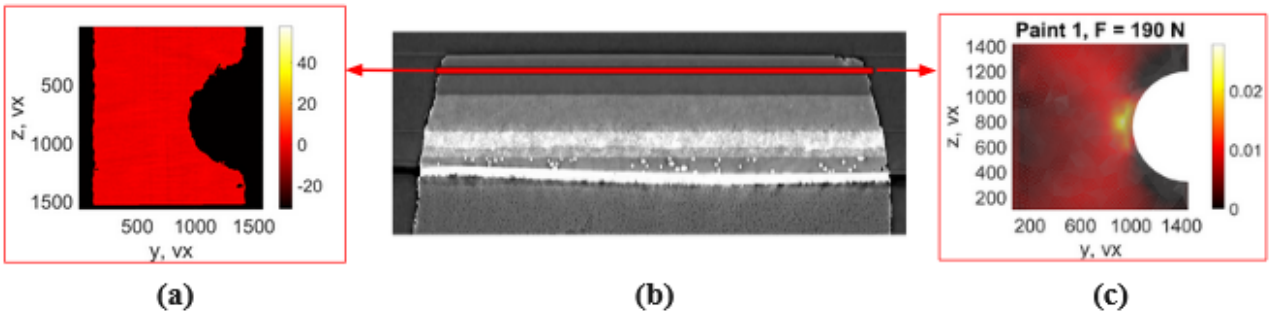


**Figure 2**: (a) Gray level residuals map. (b) View of the multilayered material focusing on the paint and copper layers. The red line shows the section of interest in the first paint layer. (c) Corresponding longitudinal strain field $\epsilon_{zz}$

## REFERENCES


[1] F. Hild, A. Bouterf, L. Chamoin, H. Leclerc, F. Mathieu, J. Neggers, F. Pled, Z. Tomičević & S. Roux. Toward 4D Mechanical Correlation. *Advanced Modeling and Simulation in Engineering Sciences*, **3(1)**:1-26, 2016.

# Hot-Wire Laser Additive Manufacturing

S. Chardin, S. Houery, C. Tournier, N. Muller

TER M1 2024-2025
Final defence of research projects

école normale supérieure paris–saclay

**TER M1 2024-2025**
FINAL DEFENCE OF RESEARCH PROJECTS
April 02, 2025, Gif-sur-Yvette, France

# Hot-Wire Laser Additive Manufacturing

**S. Chardin, S. Houery, C. Tournier, N. Muller**

Department of Mechanical Engineering
Ecole Normale Supérieure de Paris Saclay
4 Avenue des Sciences, 91190 Gif-Sur-Yvettes, France
e-mail: name.lastname@ens-paris-saclay.fr

**KEYWORDS:** Wire Laser Additive Manufacturing; Hot Wire; Design of Experiments; Process Parameters; Inconel 718; Bead Shape Analysis

The Wire Laser Additive Manufacturing (WLAM) process produces near-net-shape parts by melting a wire locally with a laser (Figure 2a). While effective with a coaxial laser as the sole power source, it remains suboptimal due to significant energy reflection from the wire and substrate. Implementing a wire preheating system [3] helps mitigate this loss, as demonstrated on Inconel 625 [2]. It should also improve bead quality and overall process efficiency [4].

The goal of this research was to determine the production parameters enabling successful fabrication: laser power, preheating current, nozzle speed, and wire feed speed. These parameters were assessed based on process robustness, bead quality, and defect prevention (e.g., dripping or stubbing). Different types of beads are shown (Figure 2b).

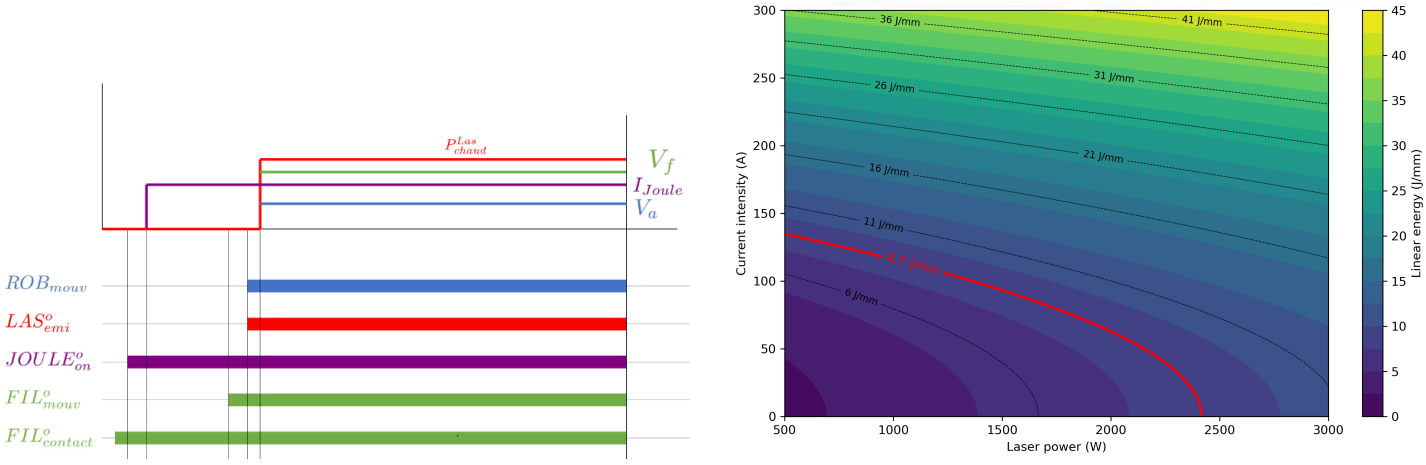


(a) Hot-Wire Production Startup Method

(b) Linear Energy at a Wire Speed of 2 m/min

Figure 1

WLAM with an hot-wire module required modifying the startup procedure (Figure 1a). Unlike cold-wire, which can start without wire-substrate contact, hot-wire requires pre-heating before the process begins, meaning the wire must be in contact with the substrate beforehand. We developed a routine to automatically detect wire-substrate contact, and to ensure robustness, a laser shot is performed beforehand to create a clean wire-substrate interface.

We then needed to identify suitable parameters for the hot-wire process. Since testing four variables was too time-consuming, we initially fixed the wire-to-nozzle speed ratio at 2, based on Roch (2024) [1], who determined that this ratio is optimal for cold-wire.

To predict outcomes, we calculated the linear energy supplied to the wire. [1] found that 8.7 J/mm was necessary for proper melting. This value is represented by the red line on the last graph (Figure 1b). While this model omits heat transfer and bead dilution effects, it streamlined our test campaign.

Experiments showed that laser power should not fall below 1500 W to ensure robustness and sufficient bead dilution. We also found that the previously used ratio of 2 was unreliable, as it risked losing wire-substrate contact. A ratio of 2.7 was found to be more stable.

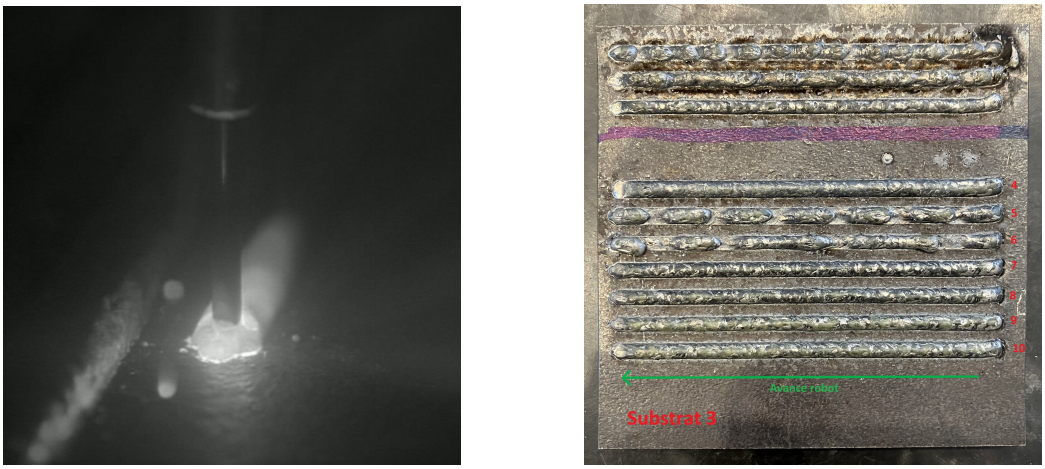


(a) Image of the process

(b) Example of beads

Figure 2

## References


[1] Clément Roch *et al.* "Intégration des spécificités d'une configuration coaxiale multi-faisceaux pour la maîtrise du procédé de fabrication additive laser-fil". Theses. Université Paris-Saclay, July 2024. URL: https://theses.hal.science/tel-04971085.

[2] Guoxing Su *et al.* "Improving the deposition efficiency and mechanical properties of additive manufactured Inconel 625 through hot wire laser metal deposition". In: *Journal of Materials Processing Technology* 322 (2023), pp. 118–175. DOI: https://doi.org/10.1016/j.jmatprotec.2023.118175.

[3] Michael Kottman *et al.* "Laser Hot Wire Process: A Novel Process for Near-Net Shape Fabrication for High-Throughput Applications". In: *JOM* 67 (2015), pp. 622–628. DOI: https://doi.org/10.1007/s11837-014-1288-1.

[4] Naksuk *et al.* "Experimental investigation of hot-wire laser deposition for the additive manufacturing of titanium parts". In: *Materials Research Express* 9.5 (May 2022). DOI: 10.1088/2053-1591/ac6ec2. URL: https://dx.doi.org/10.1088/2053-1591/ac6ec2.

# Development of an original experimental protocol for monitoring and control of damage of a mechanical structure

M. Retailleau, T. Elkaim-Weil, L. Chamoin, M. Poncelet

TER M1 2024-2025
Final defence of research projects

école normale supérieure paris–saclay

**TER M1 2024-2025**
FINAL DEFENSE OF RESEARCH PROJECTS
March $20^{th}$, 2025, Gif-sur-Yvette, France

# Abstract:
# Development of an original experimental protocol for monitoring and control of damage of a mechanical structure

**Mathieu Retailleau[1], Tessa Elkaim-Weil[1], Ludovic Chamoin[1,2], Martin Poncelet[1,2]**

[1] Département Génie Mécanique
ENS Paris-Saclay
4 Av. des Sciences, 91190 Gif-sur-Yvette
mathieu.retailleau@ens-paris-saclay.fr
tessa.elkaim–weil@ens-paris-saclay.fr

[2] Laboratoire de Mécanique de Paris-Saclay
ENS Paris-Saclay
4 Av. des Sciences, 91190 Gif-sur-Yvette
ludovic.chamoin@ens-paris-saclay.fr
martin.poncelet@ens-paris-saclay.fr

**KEYWORDS:** Experimental protocol; Prototype design; Structural Health Monitoring.


**Figure 1**: Testbed

Structural Health Monitoring (SHM) is crucial in optimizing systems maintenance. It allows for adjustments to operating conditions to prevent the propagation of cracks and, consequently, extend the systems' lifetime. Many experimental methods have been developed to perform spot check. However, continuous knowledge about structural health remains insufficient. This paper analyses an on-board system in order to have autonomous mechanical structures able to perform online monitoring of their integrity and take anticipated actions during service before downtime of failure occurs. In this study, the focus is on damage to a wind turbine blade. An original experimental protocol is developed to test the relevance of optic fibre monitoring in implementing a dynamic data-driven application systems (DDDAS) process with a global feedback loop for SHM.

An experimental platform has been designed to test a prototype wind turbine blade. This test rig incorporates a hexapod with six parallel axes [1], capable of simulating wind loads by applying forces in all directions. The prototype must reproduce as closely as possible the behaviour of a real blade made of composite material, while remaining damageable during testing. The sample consists of plaster strips applied to an intermediate 3D-printed component, the geometry of which is predefined. The number of superimposed layers is adjusted to ensure damageability suited to the forces exerted by the hexapod.

The design also includes test bed anchoring solutions to initiate the damage in the useful area. To achieve this, it is crucial to design solutions that guarantee that damage occurs solely in the valuable area of the specimen rather than at the connections between the blade and the test rig. To minimise stress concentrations, we reinforced the upper and lower sections with additional cast plaster. The lower part was plastered, leaving space for the screws, thus multiplying the stress transmission points. The connection between the tripod joint and the upper part of the blade was also created with plaster. These solutions enable stresses to be distributed across multiple zones, thereby minimizing stress concentrations.

Regarding the choice of optical fiber, it relies on its high accuracy and ability to access the measure of damage to the material, unlike conventional methods such as image correlation [2]. Fiber optics can only measure strain along the path it follows. Therefore, to identify the areas of measured deformation, it is essential to know the precise location of the fiber. We began by using photogrammetry to determine the exact geometry of the blade. From there, an optimal fibre path has been defined that allows to target the areas most likely to be subjected to high stresses. Finally, we integrated this ideal path into the UR5e robot to locate and glue the fibre along this optimal path. This robot, equipped with a laser beam, points out the exact positions where the fibre should be fixed, thus guaranteeing compliance with the determined path.

At the same time, a digital twin has been developed, integrating the data from the sensors and providing detailed monitoring of the damage evolution within the structure. This approach also allows the real-time adaptation of the forces applied by the hexapod to relieve the most damaged areas and optimize stress distribution [3].


**Figure 2**: Designed wind turbine blade

The results gathered during the design of the test specimen highlighted several key areas for enhancement. Firstly, it is preferable to pour the plaster simultaneously over all areas of the blade to avoid any risk of dehumidification, which could result in variations in mechanical properties and compromise the homogeneity of the structure. In addition, it would be interesting to reduce the rigidity of the intermediate component to prevent its melting – as the process could damage the plaster fibres due to the temperature rise. We will have to discuss the mechanical tests : the aim is to stress the blade in both torsion and bending. We will analyse the deformation under the effect of the forces applied by the hexapod. The force cells will record the forces measured, and the damage caused by these forces will be injected into the digital twin [4]. Based on the simulations, adjustments can be made to the loads applied to extend the service life of the mechanical structure.

## REFERENCES

[1] A. Carpiuc, M. Poncelet, K. Kazimirenko, H. Leclerc, and F. Hild, "A complex mixed-mode crack propagation test with a 6-axis testing machine and full-field measurements," *Eng. Fract. Mech.*, vol. 176, pp. 1-22, 2017.

[2] L. Chamoin, "DREAM-ON: merging advanced sensing techniques and simulation tools for future Structural Health Monitoring technologies," *The Project Repository J.*, vol. 10, pp. 124-127, 2021.

[3] F. Darema, "Dynamic data driven application systems: a new paradigm for application simulations and measurements," in *Comput. Sci. - ICCS 2004*, Springer, pp. 662-669, 2004.

[4] L. Chamoin, E. Baranger, A. Benady, P.-É. Charbonnel, M. Diaz, et al., "A novel DDDAS architecture combining advanced sensing and simulation technologies for effective real-time structural health monitoring," 2023, ffhal-04425882f.

# In-plane vs out-of-plane buckling of architectured materials

A.Petit, R. Gondallier de Tugny, E. Belin

TER M1 2024-2025
Final defence of research projects

école normale supérieure paris–saclay

**TER M1 2024-2025**
FINAL DEFENCE OF RESEARCH PROJECTS
March 25, 2025, Gif-sur-Yvette, France

# In-plane vs out-of-plane buckling of architectured materials

**Antoine Petit*, Raphaël Gondallier de Tugny*, Emile Belin***

* DER GM
ENS Paris-Saclay
4 Avenue des Sciences, 91190, Gif-Sur-Yvette
antoine.petit1@ens-paris-saclay.fr
rapahel.gondallier_de_tugny@ens-paris-saclay.fr
emile.belin@ens-paris-saclay.fr

**KEYWORDS:** Buckling; Compaction; Architectured Materials; Boundary Conditions.

## Context

Architectured materials, characterized by a variety of shapes and structural designs, have gained significant attention due to their mechanical properties, making them suitable for lightweight and high-strength applications in aerospace, automotive, and biomedical industries. However, their deformation mechanisms under both uniaxial and biaxial compression remain incompletely understood.

Although extensive research has been conducted on these materials, to the best of the authors' knowledge, no previous study has systematically examined how geometry, material properties, and boundary conditions interact with structural stability under such conditions. Feng Xie et al. [1] report experimental results, but their reproduction is difficult. This study aims to replicate their findings and analyze the causes of any discrepancies, which may result from a competition between in-plane and out-of-plane buckling under compressive loads.

## Methods

To achieve these objectives, a combination of experimental and computational methods was employed, building on the theoretical framework proposed by Combescure et al. [2]. Samples with different honeycomb configurations were fabricated using polymer 3D printing or elastomer molding. Uniaxial compression tests were conducted, and numerical simulations were performed to predict material behavior. Images were taken every five seconds. The clearance allowed for the specimen to buckle out of plane was adjusted to better understand the effect of this phenomenon.

To detect the appearance of in-plane buckling as a function of the images and the force curve, a code developed by Poncelet et al. [3] is modified and used. Based on a 4-part sub-windowing of the images, an indicator of the change of periodicity of the structure is calculated for each of them. The maximum variation of this indicator will then be sought in order to detect the localization of buckling and its history.

After performing compression tests, significant out-of-plane buckling was observed. The objective of the current analysis is also to detect this out-of-plane event using image correlation techniques. Vertical digital image correlation was then applied to assess the extent of vertical compression and accurately estimate the total vertical displacement.This

information was then used to interpolate the final image, aligning it vertically with the initial image. This preprocessing step enabled a subsequent horizontal image correlation, allowing the deduction of the horizontal displacement, which corresponds to the out-of-plane movement of the sample.

### Analysis of Experimental Results and Challenges

Despite using identical conditions and material configurations, the mechanical responses, such as buckling and deformation patterns, were poorly reproduced, revealing significant inconsistencies with the results reported by Feng Xie et al. [1]. These inconsistencies are likely not due to a single factor, but rather a combination of limitations in our experimental setup, variations in material properties, and differences in the fabrication process.

One of the main findings from our investigation is that previous studies do not sufficiently address out-of-plane buckling, which likely plays a significant role in influencing the results. The results of the analysis of image correlations, which is still in progress, should provide conclusions regarding the chronology of in-plane and out-of-plane buckling.

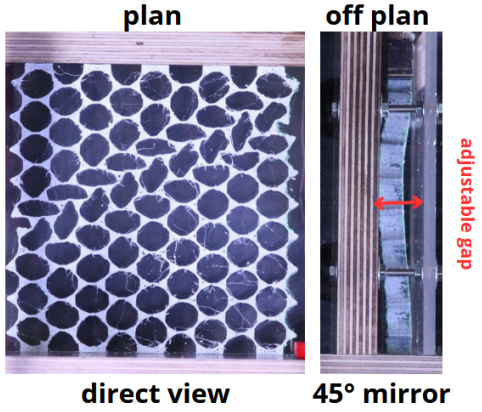


**Figure 1**: Experimental observation of in-plane and out-of-plane buckling.

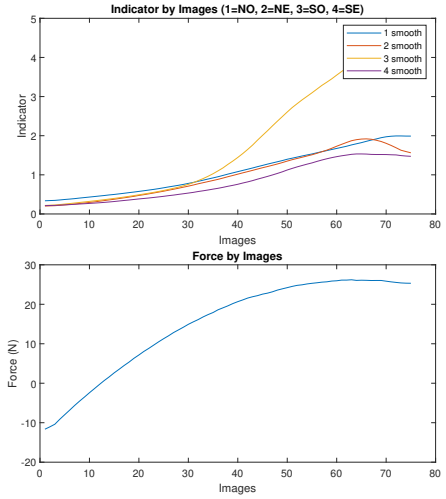


**Figure 2**: In-plane indicator results.

## REFERENCES

[1] Feng Xie et al., "Harnessing pattern transformation of honeycomb structures for soft actuators design", Composites Part B: Engineering, Volume 295, 2025.

[2] Christelle Combescure et al., "Deformation patterns and their stability in finitely strained circular cell honeycombs", Journal of the Mechanics and Physics of Solids, Volume 142, 2020.

[3] M. Poncelet et al., "Detecting bifurcations in 2D periodic metamaterials from images", Materials Letters, Volume 353, 2023.

# Experimental Learning of 3D Hyperelastic Behavior with a Physics-Augmented Neural Network

K. @mspbwmr, K. Amkn_lq* A. H_gjgl

TER M1 2024-2025
Final defence of research projects

école normale supérieure paris–saclay

# Experimental Learning of 3D Hyperelastic Behavior with a Physics-Augmented Neural Network

**M. Bourdyot*, M. Compans* C. Jailin◇**

*Génie mécanique
Université Paris-Saclay, ENS Paris-Saclay
4 avenue des sciences, Gif-sur-yvette,
91190, France

◇CNRS - LMPS
Université Paris-Saclay, CentralSupélec -
ENS Paris-Saclay - Laboratoire de
Mécanique Paris-Saclay
Gif-sur-Yvette, 91190, France

**KEYWORDS:** Physics Augmented Neural Network; Digital Volume Correlation ; 3D Material Behavior.

## Introduction

Materials behavior is essential for mechanics analysis. Classically, the response of materials is determined by theoretical thermodynamics models. This shows limits when considering complex behaviors as hyper-elasticity. With the booming of artificial intelligence, new data-driven methods of behavior identification have been developed. One recent method is the "Physic-Augmented Neural Network" (PANN), where the physical laws are included in the network architecture itself [1]. The development of digital image and volume correlations enables the collection of the deformation field required to feed the PANN. Recently, the algorithm EUCLID was developed to evaluate the equilibrium state of mater [2]. The computed stresses could be associated with strain measured, reaction forces, and the mesh constructed. These advances were used to identify a 2D hyperelastic behavior with a tensile experiment [3]. However, this approach has supposed a strong plane stress state hypothesis that limits the method's potential. The aim of this study is to extend this method to 3D digital volume correlation measurements.

## Methods

Our work aimed to identify a material's response starting from experimental 3D strain fields. These fields were computed by a mechanically regularized DVC from X-ray scans taken during an in-situ tensile test. Based on the EUCLID algorithm, a loss, $\mathcal{L}$, evaluating the equilibrium state of a stress prediction was developed.

$$\mathcal{L} = \sum_{i \in \Omega_{\text{int}}} f_i^2 + \sum_k \left[ F_k - \sum_{i \in \Omega_{\text{BC}k}} f_i \right]^2 \quad ,$$

with $f_i$ the nodal forces and $F_k$ the boundary conditions in the internal and boundary condition domains, $\Omega_{\text{int}}$ and $\Omega_{\text{BC}}$.

First approximations of the stresses in the material were estimated with a classic linear elasticity law (LE) and the Neo-Hookean (NH) whose density energy $W$ can be written from Lamé coefficient and deformation invariants:

$$W = \frac{\mu_{\text{NH}}}{2}(I-3) - \mu_{\text{NH}} \log(J) + \frac{\lambda_{\text{NH}}}{2} \log(J)^2 \quad .$$

The identified parameters are obtained from the minimization of the EUCLID loss.

The PANN architecture used has a first layer that computes, from the deformation gradient tensors, the deformation invariants $I$, $J$, $I_2$, $-J$, $(J-1)^2$, $\log(J)$ and $(\log(J))^2$. It provides entries to the 5 layers of 5 neurons with trainable weights and Softplus activation functions. Then, a layer composed of a single neuron with a ReLU activation function gives the deformation energy. Finally, stresses were computed by deriving the energy with respect to the deformation gradient tensors. An Adam optimizer with a decreasing learning rate was used to optimize the model weights. The accuracy of the model is evaluated with its loss computation.

## Data

A uni-axial tensile test has been performed on a thermo-polyurethane (FDP TPU 92A) specimen. The tensile test was controlled in displacement at $50\mu m/s$. 4 steps of 7mm were done. The sample is a 3D printed $35\times20\times110\text{mm}^3$ rectangular parallelepiped drilled at different locations to concentrate deformations zones. At

each loading step, 3D image acquisition was conducted using X-ray tomography. A 25kN load cell measured the applied force.
The dataset of 4 load steps was split into different subsets (train, validation, and test sets). The first and the fourth loading steps trained the models, and the third was used as the validation dataset.

## Results

The DVC was applied on a mesh of 20801 elements, 4537 nodes, giving 4 displacement fields for each loading step with a voxel size of 30$\mu$m. The nodal displacement field for the third loading step is shown in Figure 1. Then, the finite

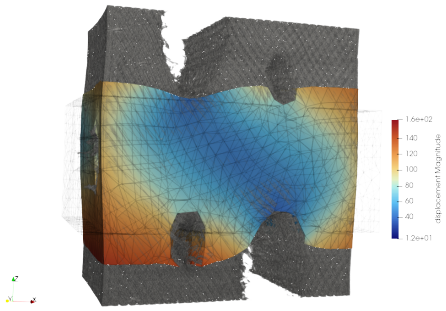

**Figure 1**: displacement field of the 3$^{\text{rd}}$ step

element gradient and divergence matrices were constructed for each element to compute the deformation fields and the nodal forces.

Using a LE and NH law, an approximation of the stress field was computed. This allows the estimation of the material parameters minimizing the EUCLID loss. Results are presented in Table 1 and evaluated an the 3$^{\text{rd}}$ step.

| Model | E (MPa) | nu | Loss valid |
|---|---|---|---|
| EL | 2.3 | 0.28 | 1299779 |
| NH | 11 | 0.34 | 3622 |
| 3D-PANN | - | - | 2942 |

**Table 1**: Results comparison between the different approaches

The unsupervised PANN model predicts a state closer to the equilibrium compared to the NH and LE models. It indicates that the law found by the algorithm better represents the real behavior of the material. It appears in both cases that the boundary conditions are visible trough the nodal forces, the top and bottom forces compensate. Moreover, with the linear elastic model that equilibrium is less respected on areas of large strain (Figure 2).

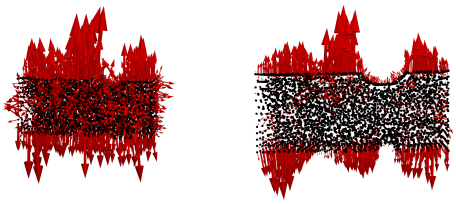

**Figure 2**: residual forces with the LE model (left) and the PANN model (right).

## Conclusion

The PANN model, trained with 3D strain fields collected using DVC and a loss function based on the EUCLID algorithm, appears to improve the accuracy of material response prediction. Further research could optimize the architecture of the PANN to find the optimal one for hyperelastic response. Moreover, experimenting with more complex behaviors, such as thermal coupling or load history, could be interesting.

## REFERENCES


[1] Lennart Linden L, Klein D K, Kalina K A, Brummund J, Weeger O and Kästner M (2023) *Neural networks meet hyperelasticity: A guide to enforcing physics.* Journal of the Mechanics and Physics of Solids 105363

[2] Thakolkaran P, Joshi A, Zheng Y, Flaschel M, De Lorenzis L, Kumar S (2022) *NN-EUCLID: Deep-learning hyperelasticity with- out stress data.* Journal of the Mechanics and Physics of Solids 169:105076

[3] Jailin C, Benady A, Legroux R, Baranger E (2024) *Experimental Learning of a Hyperelastic Behavior with a Physics-Augmented Neural Network* Experimental Mechanics

# Production multi-entité et mise à jour dynamique en WLAM par mesure in-situ des entités produites

D. Del Rey Segovia, M. Vadot, Y. Quinsat, K. Hachem†

TER M1 2024-2025
Final defence of research projects

école normale supérieure paris–saclay

**TER M1 2024-2025**
FINAL DEFENCE OF RESEARCH PROJECTS
April 2, 2024, Gif-sur-Yvette, France

# Production multi-entité et mise à jour dynamique en WLAM par mesure in-situ des entités produites

**D. Del Rey Ségovia*, M. Vadot*, Y. Quinsat†, K. Hachem†**

* Génie Mécanique
Ecole Normale Supérieur Paris Saclay
4 Avenue des Sciences 91190 GIF Sur YVETTE.
e-mail: denis.del_rey_segovia@ens-paris-saclay.fr
e-mail: maxence.vadot@ens-paris-saclay.fr

† Laboratoire universitaire de recherche en production automatisé
Université Paris Saclay
e-mail: yann.quinsat@ens-paris-saclay.fr
e-mail: khalil.hachem@ens-paris-saclay.fr

**Corection a apporter + mise en contexte + faire un seule paragraphe + décrire vite fait les méthodes et leur base de description**

**KEYWORDS:** wire-laser additive manufacturing; image correlation; defects measurement; modal basis;super-ellipsoids .

Wire-laser additive manufacturing is a process used to produce complex parts involving multi-entities. This technique involves adding metal layer by layer by melting a metal wire locally on the surface of the part. The process can vary significantly depending on the laser power and the heat distribution within the part. However, as we aim to produce increasingly larger parts with multiple entities, these defects accumulate, eventually rendering the part unusable. In order to apply a correction, a representation of the part with its defects is necessary. There are two interesting ways to do that. The first is a classic approach with a modal basis [4], the second is to fit a single super-ellipsoid. Thus, in this paper, a two-model comparison will be applied to identify the best method to use according to the geometry of the part.

In order to extract the parameters of the two representations, we used the stereo-correlation technique. It is a method for measuring a part through images by capturing two images from different points of view. Then it is possible to reconstruct the 3D geometry of the part. With further analysis, we can also identify and quantify defects in relation to the nominal design. After a calibration of the two fixed cameras' intrinsic and extrinsic parameters with a calibration target, the location of the part is ascertained by employing the mesh of its base in conjunction with photographs captured by the cameras. For the good doing of that latest operation, the distortion of the pictures have been negated and their gray gradient has been improved.Once everything is calibrated, we processed to a gradient descent.

The part used for the correlation must represent all the aspects we can find on manufactured parts using a WLAM. So we need to produce a piece of multi-entity, with a full part and a hollow part, with good and bad description of the defect for each base of defect. In our piece, we want to compare different methods of production. This is why we can divide the piece into three parts. The first is a metal filled cylinder. The second and third are two

little flyers, one straight and one twisted. As the multi-entity is still not fully mastered, the overall fabrication operation was quite difficult. Moreover, as many parameters such as the layer height and the power of the laser could cause a failure of production, a stable recipe, which can only be obtained by doing experiments, was needed.

The two cameras took photographs of the part at many angles (from 0° to 180° with a 30°interval) and with five types of mesh (no mesh, 2 speckle, and 2 circle mesh) after each fabrication step. A first selection of the picture was made to discard the ones where the visibility was not good enough on the cameras. The pictures with the best visibility were taken with a 150° and a 180° angle. Then, the results from the stereo-correlation whith these two angles were compared with the results found with an ATOS Core. For the modal basis approach, the analysis was done with five (rigid body modes and expansion mode), ten, and twenty-five modes. For a simple form such as a cylinder, the best results were obtained for the two speckle meshes and the mesh with small circles. In addition, the 150° angle gave the best overall results. Once the best analysis conditions were found, we proceeded with the other calculus. The modal analysis gave a better description of the surface of the part, but that description was only good on the visible part, meaning that the descriptions obtained for the hidden surfaces were absurd. The super-ellipsoid fitting method gave a more macro-like description of the part, but was better to depict the overall structure and accurately placed the part in the space. However, it struggled for the most complex forms, such as a twisted fin. Further experimentations could be made for a combined use of the super-ellipsoid and the modal basis description.

## 1 Annexes

## References


[1] Laurent Chevalier—Fabrice Jaillet—Atilla Baskurt. "Segmentation et modélisation 3D par un ensemble de superellipsoıdes". In: *Revue internationale d'ingénierie numérique. Volume* 1.3 (2005).

[2] David Etievant. "Une approche unifiée pour la mesure et l'analyse des défauts de forme des pièces mécaniques". Theses. Université Paris-Saclay, Nov. 2022. URL: https://theses.hal.science/tel-03988852.

[3] David Etievant et al. "A modal approach for shape defect measurement based on global stereocorrelation". In: *Optics and Lasers in Engineering* 128 (2020), p. 106030. ISSN: 0143-8166. DOI: https://doi.org/10.1016/j.optlaseng.2020.106030. URL: https://www.sciencedirect.com/science/article/pii/S0143816619315362.

[4] Khalil Hachem et al. "Modal approach based on global stereocorrelation for defects measurement in wire-laser additive manufacturing". In: *Journal of Electronic Imaging* 33.3 (2024), p. 031206. DOI: 10.1117/1.JEI.33.3.031206. URL: https://doi.org/10.1117/1.JEI.33.3.031206.

# Genetic Algorithms for Solving the Inverse Problem of Engine Performance in the Presence of Sensor Faults

R. Maison, U. Poulain
Encadrants : F. Feyel, S. Thepaut, S. Razakarivony, D. Q. Vu, G. Doquet,

TER M1 2024-2025
Final defence of research projects

école normale supérieure paris—saclay

**TER M1 2024-2025**
FINAL DEFENCE OF RESEARCH PROJECTS
April 2, 2024, Gif-sur-Yvette, France

# Genetic Algorithms for Solving the Inverse Problem of Engine Performance in the Presence of Sensor Faults

**Auteur : *U. Poulain, R. Maison***
**Encadrants : F. Feyel, S. Thepaut, S. Razakarivony, D. Q. Vu, G. Doquet,**

[*] Département de génie mécanique
Ecole Normale Superieure Paris Saclay
4 avenue des sciences 91190 Gif-sur-Yvette
e-mail: ulysse.poulain@ens-paris-saclay.fr
e-mail: romain.maison@ens-paris-saclay.fr

[†] Safran Tech
Rue des jeunes Bois, 78112 Magny-les-Hameaux France
e-mail: solene.thepaut@safrangroup.com, sebastien.razakarivony@safrangroup.com,
guillaume.doquet@safrangroup.com, dong-quan.vu@safrangroup.com

**KEYWORDS:** Genetic algorithm; sensor fault detection; inverse problem.

## ABSTRACT

### Context and Introduction

Modern aeronautical engines require precise monitoring to ensure high reliability and efficient operation. Predictive maintenance often involves estimating internal parameters (or health indicators) that reflect the overall condition of the engine, through the health status of its different modules (such as the compressor and turbine). These parameters are typically not measurable during operation, which leads to an inverse problem: estimating the engine's internal condition from available sensor measurements using a gas turbine model.

Historically, solutions have relied on Gas Path Analysis (GPA) [2], neural networks[1], and Kalman filters [7]. Despite their usefulness, these methods often rely on strong assumptions (e.g., linearity or differentiability) or require extensive datasets for training. Furthermore, they may struggle with under-determined systems, where multiple internal states correspond to the same sensor observations [1].

Genetic Algorithms (GAs) are optimization methods inspired by biological evolution [6], [3]. They iteratively improve a set of candidate solutions (population) by evaluating their quality (fitness), selecting the best individuals, and generating new solutions through crossover and mutation. Unlike gradient-descent-based approaches, GAs allow for a broader exploration of the solution space. This makes them particularly well-suited for inverse problems involving ambiguity or redundancy, and they are promising tools for applications such as sensor fault detection [8], [4]—although this aspect is only briefly introduced in our current work. Sensor fault detection has been addressed in the literature through various approaches, including statistical models, neural networks, and Kalman filters, each offering advantages and limitations depending on the type and severity of faults [5], [9]. Our simulator is specific as it includes the possibility of modeling sensor faults explicitly, a feature that remains relatively rare in the literature.

## Methodology

Our approach uses the PyGAD Python library to implement a GA framework. Each candidate solution encodes engine health parameters and a Boolean variable indicating the presence of a sensor fault. The fitness function evaluates the match between simulated and observed outputs ($P_3$, $T_4$), defined as:

$$\text{fitness} = -\left(\left|\frac{P_{3,\text{target}} - P_{3,\text{sim}}}{P_{3,\text{target}}}\right| + \left|\frac{T_{4,\text{target}} - T_{4,\text{sim}}}{T_{4,\text{target}}}\right|\right) \times 1000$$

Selecting an appropriate fitness function is a critical and non-trivial task, as it strongly influences convergence and robustness. We use steady-state selection, adaptive crossover, and Gaussian mutation to explore the parameter space efficiently while maintaining solution diversity. Multiple runs are performed to ensure reproducibility and assess the algorithm's sensitivity to initialization.

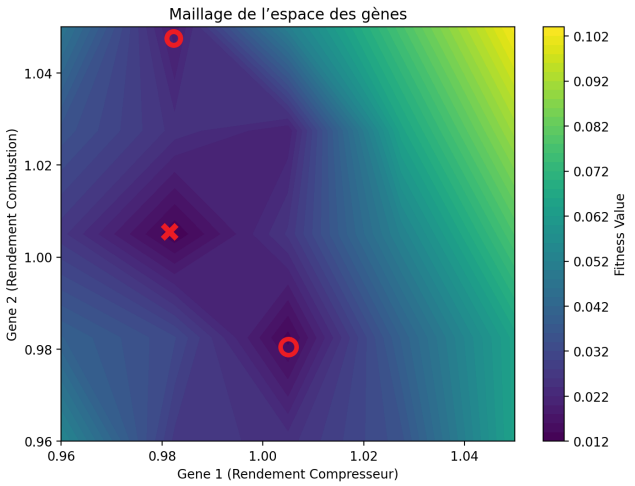


**Figure 1**: Fitness function heat map. The figure shows two optima: the correct one is marked with a cross, while convergence states reached by the algorithm under different scenarios are shown as circles. This illustrates the difficulty of distinguishing between sensor faults and healthy states.

## Key Results

Initial tests on a simplified engine model demonstrated that our GA approach efficiently explores complex, non-convex parameter spaces and avoids local minima. The algorithm successfully recovers plausible health indicators and highlights multiple valid optima, including those resulting from potential sensor faults. While promising, the approach remains computationally expensive for large-scale problems, motivating future improvements such as parallelization or surrogate modeling.

The integration of sensor fault indicators within the optimization process represents a first step toward robust health monitoring under faulty measurement conditions. Further work is required to validate these capabilities in more realistic scenarios explicitly involving known sensor faults.

## Conclusions and Perspectives

Genetic Algorithms offer a robust, flexible approach for engine health monitoring, particularly in underdetermined settings. Our results demonstrate their potential for estimating health parameters and handling ambiguity induced by measurement faults.

## References


[1] De Giorgi & Quarta (2020). Hybrid GP-ANN for aeroengine prediction. *Aerosp. Sci. Technol.*, 103.
[2] Fentaye et al. (2019). Review on GT gas-path diagnostics. *Aerospace*, 6(7).
[3] Li et al. (2011). GT off-design adaptation via GA. *JEGTP*, 133(7).
[4] Li (2017). GT sensor fault diagnosis using GA. *Aeronaut. J.*, 121(1242).
[5] Deb et al. (2002). NSGA-II algorithm. *IEEE Trans. Evol. Comput.*, 6(2).
[6] Mitchell (1998). *Intro to Genetic Algorithms*. MIT Press.
[7] Simon (2006). Hybrid Kalman Filter for engine diagnostics. NASA.
[8] Zedda (n.d.). GT engine & sensor fault diagnosis.
[9] Manzoni et al. (2021). Fitness function for engine health. *J. Propuls. Power*, 37(5).

# Investigating the influence of graphene coating on the mechanical properties of pineapple leaf fibers

J. PARVERY , B. BOUCHOT , C. HA-MINH

TER M1 2024-2025
Final defence of research projects

école normale supérieure paris–saclay

**TER M1 2024-2025**
FINAL DEFENCE OF RESEARCH PROJECTS
March 25, 2025, Gif-sur-Yvette, France

# Investigating the influence of graphene coating on the mechanical properties of pineapple leaf fibers

**Jeanne PARVERY*, Benjamin BOUCHOT*, Cuong HA-MINH◇**

* Department of Mechanical Engineering
Ecole Normale Supérieure Paris-Saclay, Paris-Saclay University, France
e-mail: jeanne.parvery@ens-paris-saclay.fr
e-mail: benjamin.bouchot@ens-paris-saclay.fr

◇ Université Paris-Saclay, CentraleSupélec, ENS Paris-Saclay, CNRS,
LMPS - Laboratoire de Mécanique Paris-Saclay, 91190, Gif-sur-Yvette, France
e-mail: cuong.ha-minh@ens-paris-saclay.fr

**KEYWORDS:** graphene coating; natural fiber; pineapple leaf fiber; PALF mechanical properties.

## ABSTRACT

### Introduction

To minimize the environmental impact of composites, research is being conducted on natural fiber based composites. However, the mechanical properties of such materials are strongly influenced by the properties of the natural fibers. Among various natural cellulosic fibers, pineapple leaf fibers (PALF) are a promising candidate with wide availability and low production cost [3]. It has been found that the mechanical properties of natural fibers such as PALF are significantly inferior to those of synthetic fibers such as carbon or aramid fibers. As a consequence, natural fiber-based composites are not viable as a substitute for classical synthetic composites. A novel approach has been proposed to address this challenge, involving the coating of natural fibers with graphene oxide (GO). However, the effectiveness of this approach in enhancing the mechanical properties of natural fibers remains to be fully validated. In this study, the impact of graphene coating on the Young's modulus of the pineapple fiber will be investigated.

### Materials and Methods

*Samples preparation*

In order to evaluate the influence of graphene coating on the Young modulus of PALF, four batches of 30 samples each have been prepared : one without GO coating (OD), one with one coat of GO (1D), one with two coats of GO (2D) and one with three coats of GO (3D). First, the pineapple fibers have been chemically treated with a Na0H solution in order to remove non cellulosic component and if needed have then been coated with a graphene oxide solution concentrated at 1 %. One coating operation consist of submerging the fibers for 30 seconds in the graphene oxide solution and to let it dry until the mass of the fiber no longer evolve. In order to lay multiple GO coats on the fiber, the previous operation have been repeated as many times as needed. The fibers have then been stored in a closed box with desiccant packets to remove moisture.

*Experiments*

Following the ASTM-C1557 standards [2], each fiber sample have been glued on a paper mounting tab in order to conduct tensile tests using an INSTRON 5544 testing machine equipped with a 2530-100N load cell. The experimental protocol to determine the tensile strength and the Young's modulus of the fibers has been based on the STM-C1557 standards [2] and has been validated with glass fiber testing. The four varieties of PALF were then tested with the same experimental protocol. To limit the influence of the random behavior of natural fibers, 20 specimens of each batches of fiber have been tested and the results averaged to provide an average Young's modulus value for each type of fiber. Each sample diameter was measured at five different locations with an optical microscope and averaged. The fibers were characterized using X-Ray diffraction (XRD) on a PANalytical Aeris diffractometer and Scanning Electron Microscopy (SEM) with an Hitachi S-3400N microscope.

### Results and Discussions

*Tensile test*

The results (figure 1) reveal that the GO coating has not an important impact on the Young's modulus of the fiber: 20573 $MPa$ for the 0D, 18423 $MPa$ for the 1D, 22754 $MPa$ for the 2D and 22726 $MPa$ for the 3D with a standard deviation of 30% for each value. Values were determined with the first points (red zone in figure 2) when the fiber has an elastic response. The results from the tensile tests have also provided information about the mean strain at break for each type of fiber. It appears that the OD fibers has a mean strain at break of 0.0285 while the other types of fibers have a mean strain at break of 0.0288. It seems that the GO coating

reduces the value range of strain at break and that it could increase the fragile behavior of the fibers. After the tests, an improvement of the mechanical proprieties with GO coatings was expected but no clear conclusion can be drawn and the results may be questioned. Firstly, the experimental process for the application of GO to fibers remains to be perfected in order to control the thickness of the GO layer. During the immersion in the graphene solution, ultrasonic vibration was not realized. Graphene might not perfectly integrate with fibers. Another explanation could be a lack of rigor in conducting the experiments, particularly when handling the fibers without gloves and keeping the fibers in a dry but uncontrolled environment. The variability of the structure may cause the various results obtained with the same type of fiber in the same conditions.

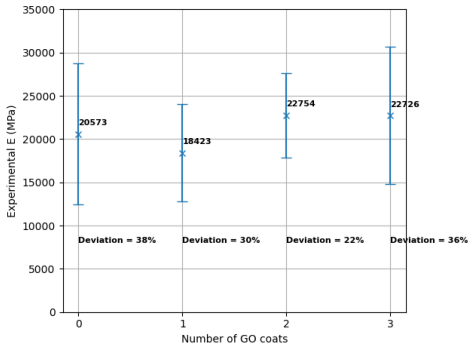


**Figure 1**: Young's modulus results obtained from the tensile tests.

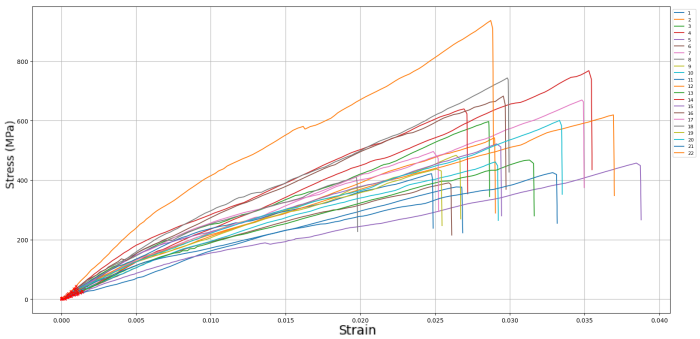


**Figure 2**: Stress-strain plots from tensile tests on 2D pineapple fibers.

Tensile tests were conducted on various fibers, the results of which are presented in figure 2 for 2D pineapple fibers. The general appearance is the same for the different numbers of GO layers deposited. This enables the typical behavior of natural fibers during a tensile test to be identified. Initially, the stress rises proportionally to the strain, indicating an elastic response. Subsequently, a number of microfibers begin to degrade and a decrease in stress is observed. Finally, once a critical number of microfibers have been broken, the fiber breaks.

*Rupture with Scanning Electron Microscope (SEM)*

The Scanning Electron Microscope was used to study the mechanisms of the bursting of the fiber. Comparing the rupture of various fibers, a traditional rupture associated to a classic Young's modulus is characterized by straight and sightly flared out microfibers at the rupture. Images taken with the SEM illustrate the peeling and degradation of the microfibers caused by the rupture [1].

*X-ray diffraction (XRD)*

The XRD analysis revealed that the fibers are composed of cellulose with peaks at 15.5° and 23°. As B.Focher et al. demonstrated, the result was expected as the fibers are natural [4].

## Conclusions

The results of the experiments carried out as part of this study underline the uncertain behavior of natural materials such as pineapple leaf fibers. As long as those uncertainties are not reduced, it will not be possible to use bio-sourced materials such as natural fibers in high-risk industries such as aeronautics. It is therefore necessary to expand the general knowledge of these materials. As part of this study, it would also be interesting to investigate other properties such as the coefficient of friction, tenacity, dynamic Young's modulus as well as lateral compression and flexural modulus.

## References

[1] Flavio de Andrade Silva, Nikhilesh Chawla, and Romildo Dias de Toledo Filho. "Tensile behavior of high performance natural (sisal) fibers". In: *Composites Science and Technology* 68.15-16 (2008), pp. 3438–3443.

[2] ASTM C1557-14. *Standard test method for tensile strength and young's modulus of fibers*. 2014.

[3] Diego M Chaves et al. "Extraction, characterization and properties evaluation of pineapple leaf fibers from Azores pineapple". In: *Heliyon* 10.4 (2024).

[4] B Focher et al. "Structural differences between non-wood plant celluloses: evidence from solid state NMR, vibrational spectroscopy and X-ray diffractometry". In: *Industrial Crops and Products* 13.3 (2001), pp. 193–208.

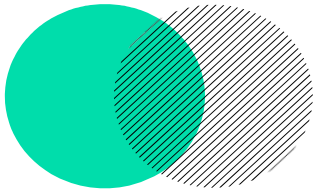

**Pierre-Louis VERLY, Bastien JACQUES, supervised by Yoann GUILHEM**

TER M1 2024-2025
Final defence of research projects

école normale supérieure paris—saclay

# Abstract
# for the Final Defence of Research Project

**Pierre-Louis VERLY, Bastien JACQUES, supervised by Yoann GUILHEM**

[*] Mechanical engineering department, Ecole Normale Supérieure
Paris-Saclay University
Laboratoire de Méchanique Paris-Saclay, Ecole Normale Supérieure - Ecole Centrale Supélec - CNRS
bastien.jacques@ens-paris-saclay.fr

[†] Mechanical engineering department, Ecole Normale Supérieure
Paris-Saclay University
Laboratoire de Méchanique Paris-Saclay, Ecole Normale Supérieure - Ecole Centrale Supélec - CNRS
pierre-louis.verly@ens-paris-saclay.fr

[◇] Laboratoire de Méchanique Paris-Saclay, Ecole Normale Supérieure - Ecole Centrale Supélec - CNRS
Paris-Saclay University
yoann.guilhem@ens-paris-saclay.fr

**KEYWORDS:** Polycrystalline networks; Convolutional Neural Network (CNN); Von Mises stress; U-net; Crystal Plasticity Finite Element Method (CPFEM).

## ABSTRACT

## Introduction

Several studies [2] [1] have highlighted a connection between the three-dimensional microstructure and the formation of fatigue cracks. Among the influencing factors are the Schmid factor, the grain's position relative to the surface, its shape, as well as its neighborhood, among others. The impact of these parameters (and possibly others) on the fatigue life of polycrystals can be analyzed experimentally, but this approach quickly becomes very costly, preventing the incorporation of statistical variability. An alternative method involves numerical simulation using the Crystal Plasticity Finite Element Method (CPFEM). This approach allows the testing of various parameter configurations influencing fatigue life, but it too remains computationally expensive.

A final approach consists of predicting the mechanical response under different loading conditions using machine learning—this is the method we will focus on in the following.

## Methods

The success of learning-based mechanical response prediction for polycrystals under different loading conditions relies heavily on the quality and diversity of the dataset. This dataset is built from CPFEM simulation results computed on synthetic 40-grain structures with a resolution of 64×64 pixels, generated using the NEPER software.

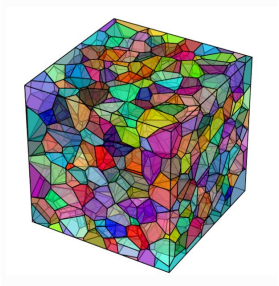

**Figure 1:** Synthetic 3D polycrystal generated using Neper

The database is constructed to include: 100 different geometries, 100 different grain orientation sets, and 100 different loading conditions (including zero loading). Thus, the dataset consists of $10^6$ unique configurations combining geometry, orientation, and loading.

For each of these configurations, we provide the machine learning model with: the 4 components of the quaternion representing the orientation of each grain (for every pixel) and the applied loading—these are the input features (X). The output (Y) to be predicted is the Von Mises equivalent stress at each pixel, which serves as the label in this supervised learning task. The geometry is implicitly known through the orientation of each grain. To improve the neural network's performance, a future version could include the distance of each pixel to the nearest grain boundary.

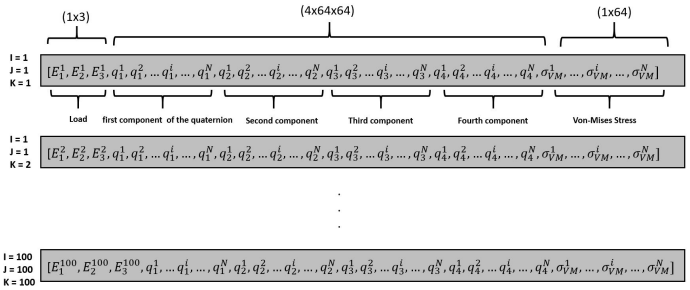


**Figure 2:** Dataset structure

We used a convolutional neural network with a U-net architecture, which belongs to the family of encoder-decoder networks. It operates in two main phases:

The first phase is the encoding phase, where the model uses successive convolutional layers with ReLU activation (ReLU(x) = max(0, x) introduces non-linearities) and pooling layers to extract features from the input image. This process results in a compression of information, where the extracted features become increasingly abstract as the image size decreases.Each convolution is performed using 16 filters in parallel, all with kernel sizes of (3×3). The output image retains the same dimensions after each filter. The max pooling operation uses a (2×2) kernel that slides over the image and keeps only the maximum value within each kernel window, thereby reducing the image size by a factor of 4.

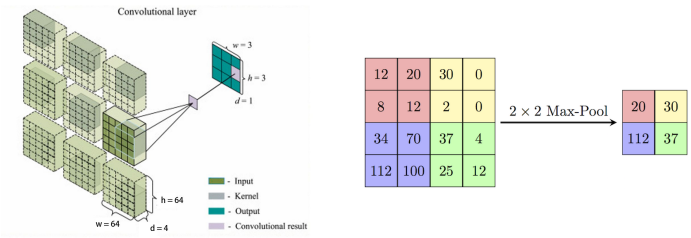


**Figure 3:** Illustration of two key components of the encoder: (left) convolutional layer and (right) max pooling layer. (Wikipédia)

Once encoding is complete, the loading parameters corresponding to each case are added. To do this, we concatenate the loading vector with the feature map obtained at the end of the encoding phase.

The second phase is the decoding phase. Here, the model uses transposed convolutions to progressively upsample the image.

A key characteristic of the U-net is its use of skip connections between the encoder and decoder paths: at each level, the features from the encoder are copied

and concatenated with those in the decoder. These skip connections help recover fine details lost during the encoding process, thereby greatly improving the spatial accuracy of the output.

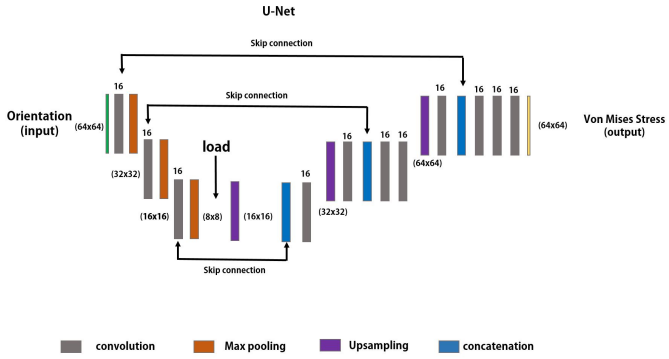


**Figure 4:** U-net structure

Batch normalization layers are also added after each layer to normalize the activations across each batch, stabilizing and accelerating the training process.For every batch output from a convolutional layer, Batch Normalization enforces the following transformation:

$$\hat{x}_i = \frac{x_i - \mu_B}{\sigma_B} \tag{1}$$

Where: $x_i$ is the activation of the $i^{th}$ example in the batch, $\mu_B$ and $\sigma_B$ are the batch mean and standard deviation. This results in a normalized distribution where:

$$\mu_{\hat{B}} = 0 \quad and \quad \sigma_{\hat{B}} = 1 \tag{2}$$

The goal of training is to minimize the MSE (Mean Squared Error) loss function. The minimization of the loss function, and thus the optimization of the model's weights and biases, is performed using the Adam optimizer, which carries out gradient descent with an adaptive learning rate based on both the momentum (the moving average of gradients) and the scale of updates (the moving average of squared gradients).

The training is carried out over 100 epochs with batches of size 32.We use a batch size of 32 as it allows for stable learning, converges quickly, and uses less RAM compared to training without batching. We can then observe the evolution of the loss functions during both the training and validation phases:

## Results

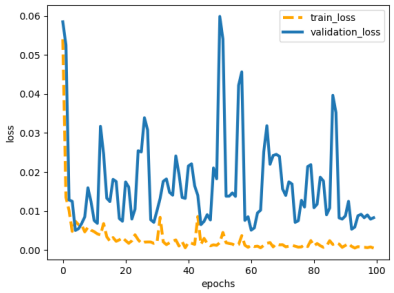


**Figure 5:** Evolution of the train loss and the validation loss with epochs

It can be observed that the validation loss is highly noisy. This may be explained by the small amount of data allocated to the validation set; as a result, the loss value varies significantly with each new epoch. At this stage, the model is not reliable enough for practical use. A larger dataset is required to obtain satisfactory results. We plot the validation loss and training loss curves to monitor and prevent overfitting. Indeed, while training is performed on the training dataset, the model is simultaneously evaluated on the validation set. If the validation loss starts to increase, it indicates that the network is overfitting, and continuing the training may harm overall performance.

## conclusion

A larger and more diverse dataset is required to obtain satisfactory results. It will also be necessary to randomize the distribution of loading cases, geometries, and orientations in order to achieve better performance.

## REFERENCES


[1] H. Proudhon R. A. Lebensohn W. Ludwig et al A. Rovinelli, Y. Guilhem. Assessing reliability of fatigue indicator parameters for small crack growth via a probabilistic framework. *Modelling and Simulation in Materials Science and Engineering*, 2017.

[2] F. Curtit J.M. Stephan G. Cailletaud Y. Guilhem, S. Basseville. Investigation of the effect of grain clusters on fatigue crack initiation in polycrystals. *International Journal of Fatigue*, 2010.

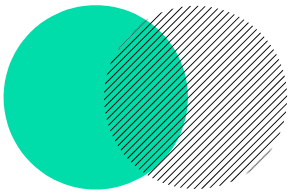

# Implementation of cyber-attack detection algorithms in an automated production system

E. Reniaud, C. Ahmidach, R. Thibert, G. Faraut

TER M1 2024-2025
Final defence of research projects

école normale supérieure paris–saclay

# Implementation of cyber-attack detection algorithms in an automated production system

**E. Reniaud*, C. Ahmidach*, R. Thibert†, G. Faraut†**

* DGM,ENS Paris Saclay
4 Avenue des sciences,91190 Gif-sur-Yvette
e-mail: prenom.nom@ens-paris-saclay.fr

**KEYWORDS:** Cyber-attack; DES; cybersecurity.

## 1 Context and related works

This project falls within the paradigm of Discrete Event Systems (DES) diagnosis [1]. These methods detect faults by comparing observed system behavior with predictions from a predefined model, similar to a medical diagnosis. Initially, they were used to detect production line failures and support maintenance operations [2].
Since the appearance of the Stuxnet virus in 2010, cyber-attacks have become a growing concern in industrial systems. Recent studies have adapted DES diagnosis to account for such threats [3,4]. In this context, attacks are modeled as event insertions or deletions in communication channels between the system and its controller. More advanced attacks may involve timing manipulations or event masking, such as hiding the detection of a person by an elevator's floor sensor.
However, current methods do not clearly distinguish between faults and attacks. This TER aims to explore strategies to make this distinction possible.

## 2 Method

To work on cyber-attacks, the nominal non-faulty language of a Bosch production line — which sorts gears and classifies them based on their material, with the possibility of inserting a plain bearing among the gears — has been identified from a previous experimental campaign. We developed a Python program that reads input/output vectors (I/O vectors) in real time and sends them to a C# algorithm, based on Schneider's work in [4], which checks whether the observed behavior conforms to the previously identified language or if a fault has occurred, and if so, which one. The C# algorithm has been modified to run two models in parallel: the original nominal model and a self-correcting model designed to closely reflect the new behaviors observed on the production line. Figure 1 presents this dual-model architecture, where the system sends I/O vectors to both models. The nominal model detects deviations from expected behavior, while the self-correcting model adapts to persistent faults. Comparing both outputs enables the distinction between regular faults and abnormal behavior potentially linked to cyber-attacks.

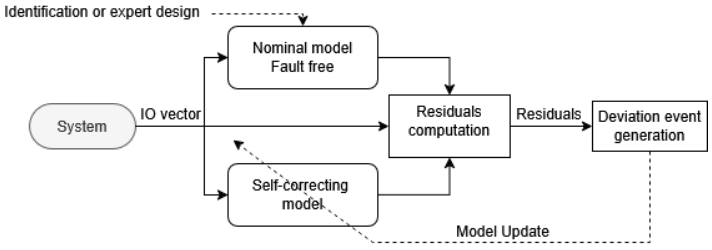


**Figure 1**: Attack Detection Method

## 3 Example of Fault Detection

Figure 2 illustrates a fault detection scenario based on a Non-Deterministic Autonomous Automaton with Outputs

(NDAAO). Along the top of the figure, a sequence of input/output (I/O) observations is shown over time, represented by vectors such as (1 0), associated with specific I/O labels like $IO_1\_0$ or $IO_2\_1$. Each observation is processed and mapped to a set of possible states $\hat{X}_i$ in the automaton. In the fault diagnosis (FD) row, the system identifies each time step as either "OK", "fault" or "attack".
The error in Figure 2, located in the bottom part representing the NDAAO, occurs due to an unexpected observation at the 5th time step. Specifically, the observation (1 0) with label $IO_2\_0$ leads to an empty set of possible states $\hat{X}_i = \emptyset$, indicating that this behavior cannot be explained by the model.
However, in our approach, the self-correcting model assumes that the sensor corresponding to the second component of the I/O vector is faulty. As a result, it treats this sensor as permanently stuck at value 1. Therefore, all expected outputs are modified to integrate a fixed 1 in the first component of the observation vectors. This change is reflected in all states of the automaton, as illustrated in Figure 3, allowing the model to accept observations that would otherwise be flagged as faults. That said, our model doesn't accept a faulty component to become not faulty therefore at the final time step, an attack is detected

| **I/O vector observed** | 1<br>0 | 0<br>0 | 1<br>0 | 1<br>1 | 1<br>0 | 1<br>0 | 1<br>1 | 0<br>0 |
|---|---|---|---|---|---|---|---|---|
| **Possible states** $Aut_{nom}$ | $\{x_1, x_3\}$ | $\{x_2\}$ | $\{x_3\}$ | $\{x_4\}$ | $\emptyset$ | $\{x_1, x_3\}$ | $\{x_4\}$ | $\{x_6\}$ |
| **Possible states** $Aut_{cor}$ | $\{x_1, x_3\}$ | $\{x_2\}$ | $\{x_3\}$ | $\{x_4\}$ | $\{x_6\}$ | $\{x_3\}$ | $\{x_4, x_5\}$ | $\{x_6\}$ |
| **Fault Diagnosis** | **Fault** | **OK** | **OK** | **OK** | **Fault** | **Fault** | **OK** | **OK** |
| | **Fault** | **OK** | **OK** | **OK** | **OK** | **OK** | **Fault** | **Attack** |

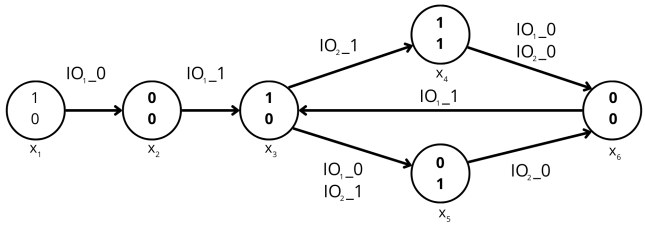


**Figure 2**: $Aut_{nom}$

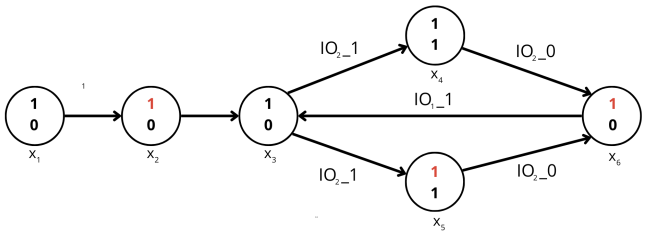


**Figure 3**: $Aut_{cor}$ after 5th time step

## 4 Conclusion

At the end of this project, we successfully produced comprehensive documentation of the Bosch production line, clearly identifying which sensors correspond to which input/output (I/O) vectors. This mapping was essential to ensure accurate monitoring and diagnosis of system behavior.
We also updated the sensor-reading Python code to align with the actual I/O structure of the production line. Furthermore, we improved the C# interfacing code by implementing a dual-automaton architecture.

## 5 Perspectives

Future research should integrate timing considerations and explore adaptive diagnosis methods in order to account for timing discrepancies between operations. Additionally, structural modifications could be taken into account for better results. Last, creating a new model for each fault, rather than a unique self-correction one, could bring better results.

## REFERENCES


[1] C. G. Cassandras et S. Lafortune, Introduction to Discrete Event Systems. Cham: Springer International Publishing, 2021
[2] M. Roth, J.-J. Lesage, et L. Litz, The concept of residuals for fault localization in discrete event systems , Control Engineering Practice, vol. 19, no 9, p. 978 988, sept. 2011.
[3] S. Oliveira, A. B. Leal, M. Teixeira, et Y. K. Lopes, A classification of cybersecurity strategies in the context of Discrete Event Systems , Annual Reviews in Control, vol. 56, p. 100907, 2023.
[4] Schneider et al. - 2011 - Timed residuals for fault detection and isolation

# Impact of the machine dynamics on PBF-LB thermals effects

Q. DUVAL, L. OTALORA, K. GODINEAU

TER M1 2024-2025
Final defence of research projects

école normale supérieure paris–saclay

# Impact of the machine dynamics on PBF-LB thermals effects

**Quentin DUVAL*, Loïs OTALORA*, Kévin GODINEAU †**

* Department : Génie Mécanique
University : École Normale Supérieure Paris-Saclay
Address : 4 avenue des Sciences, 91190 Gif-sur-Yvette
e-mail : quentin.duval@ens-paris-saclay.fr
e-mail : lois.otalora@ens-paris-saclay.fr

† Lab : LURPA
University : École Normale Supérieure Paris-Saclay
Address : 4 avenue des Sciences, 91190 Gif-sur-Yvette
e-mail : kevin.godineau@ens-paris-saclay.fr

**KEYWORDS:** Additive Manufacturing; PBF-LB; Heat Science; Dynamic behavior; Trajectory.

## Part 1: Presentation of the process and associated issues

Powder Bed Fusion - Laser Beam (PBF-LB) is a metal additive manufacturing process that consists of producing a 3D part layer by layer by fusing metal powder with a laser. However, the manufacturability, the geometry and the material health of parts is disturbed by residual stresses and deformations, directly linked to thermal gradients, which appear during manufacture [1][2]. The literature shows that these defects vary according to the type of filling trajectory used. For example, they are reduced by using small scan vectors [3][4].

Another phenomenon occurs when there is a change of trajectory, because the speed of the laser decreases due to the dynamics of the machine. Thus, the trajectory is rounded, which can amplify the previous thermal problems [5]. However, no article has studied the two problems simultaneously, i.e. the influence of the machine dynamics on the thermal effects.

The aim of this study is therefore to identify the formation of these defects as a function of the filling trajectory and then to study the impact of the machine dynamics on the PBF-LB thermics.

## Part 2: The Flash simulation method and its calibration

For this study, an analytical thermal simulation approach, known as the flash method [2], was used. In contrary to finite element methods, this simulation provides sufficient results at low computational cost. It can simulate trajectories for one layer and returns a thermal map for each instant in time. In addition, it takes into account the influence of the machine's dynamics on the trajectory, unlike the methods developed in the literature. However, it contains some simplifications, for example it only considers the fused metal and not the properties of the powder [2].

The simulation was first calibrated using experimental tests. This enabled two parameters to be identified, including the absorptivity of the material. To do this, several cords were produced by varying the speed and power of the laser. Then the simulation was adjusted according to the 2 parameters so that it was as close as possible to the experimental results.

## Part 3: Analysis of results

After calibration, different types of laser trajectory were simulated using the Flash method, such as the uniaxial, biaxial, zig-zag and zig-zag column strategies, which are classic PBF-LB trajectories.

For each simulation, a thermal map representing the maximum temperature reached at each point in the layer is obtained. In order to identify possible thermal constraints, two criteria have been chosen [1][2], based on the temperature gradient. The first is a local criterion at each point in the layer and the second is a global criterion at the scale of the layer.

When the trajectory changes, a significant temperature gradient is observed. Thus, when the dynamics of the machine are taken into account, and short scan vectors are performed, the temperature gradients are greater than when long scan vectors are performed, which contradicts the literature.

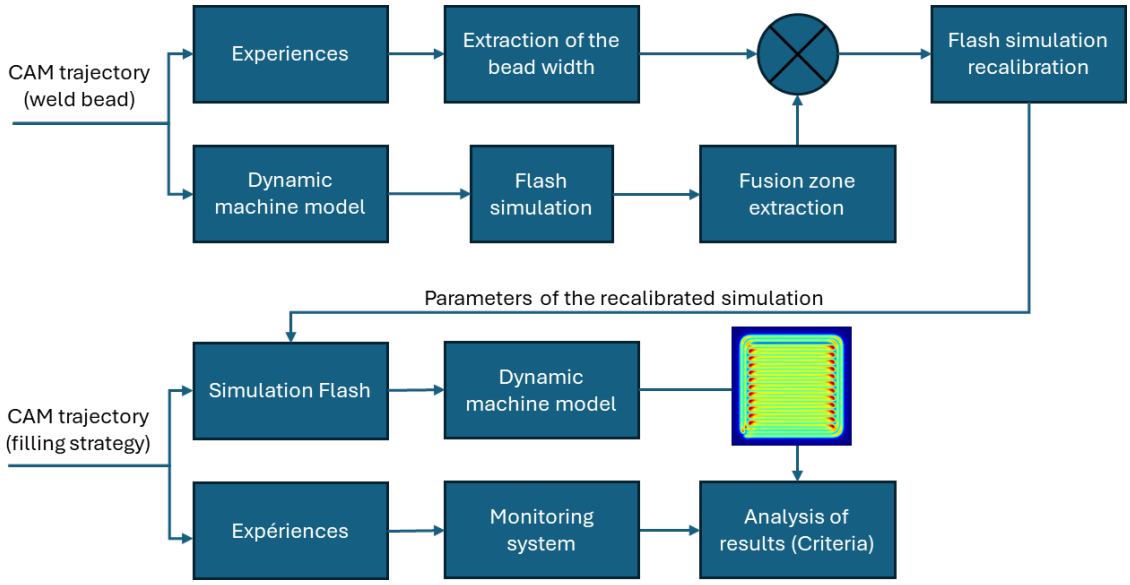


**Figure 1** : Diagram of the study.

## REFERENCES

[1] Pramod R. Zagade, B.P. Gautham, Amitava De, Tarasankar DebRoy, Analytical modelling of scanning strategy effect on temperature field and melt track dimensions in laser powder bed fusion. Additive Manufacturing, Vol 82, 2024.

[2] Kamel Ettaieb, Sylvain Lavernhe, Christophe Tournier. A flash-based thermal simulation of scanning paths in LPBF additive manufacturing. Rapid Prototyping Journal, Emerald, 2021.

[3] L. Parry, I.A. Ashcroft, R.D. Wildman, Understanding the effect of laser scan strategy on residual stress in selective laser melting through thermo-mechanical simulation. Additive Manufacturing, Vol 12, Part A, 2016.

[4] Jia, H., Sun, H., Wang, H. and al. Scanning strategy in selective laser melting (SLM): a review. Int J Adv Manuf Technol 113, 2021.

[5] Kevin Godineau, Sylvain Lavernhe, Christophe Tournier. Influence of the CNC behaviour on the laser spot trajectory in LPBF process. Joint Special Interest Group meeting between euspen and ASPE Advancing Precision in Additive Manufacturing, Sept 2021, St Gallen, Switzerland.